ACS OMEGA

http://pubs.acs.org/journal/acsodf

Article

Density Functional Theory Study of Metallic Silicon (111) Plane Structures

Chih Shan Tan*

Cite This: *ACS Omega* 2022, 7, 5385−5392

Read Online

ACCESS | Metrics & More | Article Recommendations | Supporting Information

ABSTRACT: The band structure on the surface might be influenced by the abruptly ended periodic structure and change the physical properties of the semiconductor. By using the density functional theory, this research also demonstrates that the Si unit cell has the calculated room-temperature electrical conductivity as 4.01×10^{-6} (Ω^{-1} cm^{-1}), similar to the experimental result. Thus, the Si(111) plane structures are calculated, and we found out that the one-layer and two-layer plane structures have the theoretical room-temperature electrical conductivities as 129.68 (Ω^{-1} cm^{-1}) and 547.80 (Ω^{-1} cm^{-1}), respectively. In addition, the results reveal that the conduction band and valance band of the Si(111) one-layer and two-layer structures will connect on the ⟨111⟩ direction, mainly contributed by Si 3p orbitals. Thus, the band structure at the ⟨111⟩ direction on the Si(111) surface has variation and increases the electrical conductivity to 7 to 8 orders compared to the intrinsic Si and offers new surface science and surface engineering concepts for future applications.

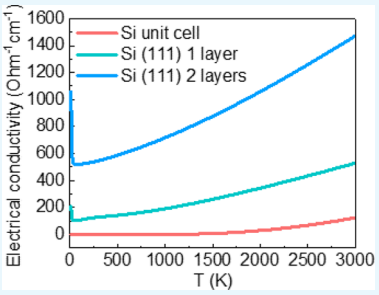

INTRODUCTION

The surface reveals the abnormal physical and chemical phenomena within the atomic world and navigates future nanotechnology development by changing the electronic behavior within the nanoscale for different material properties.[1,2] Even the surface could be measured by tremendous measurement techniques, such as electron microscopy,[3] synchrotron radiation,[4] probe microscopy,[5] and photoelectron spectroscopy;[6] moreover, theoretical calculation results could offer another atomic-scale prospect to increase the knowledge of the surface. The density functional theory (DFT) has valuable accuracy within the atomic scale for solving the issues of the electronic structure of solids.[7−11] The atomic-scale bonding variations at the surface might change the band structure behavior by verifying the periodic atom structure, especially the abruptly ended regular structure at the surface, and forming unique material properties compared to bulk materials.

Indeed, the surface plays a vital role in the nanoeffect because the regular atom arrangement must end and distort at the surface, and every material has its surface. With or without shape control, nanoparticles have a substantial electronic variation from the bulk material due to the ultrashort periodic atom range near the surface so that the surface effect could be enlarged in nanomaterials. Therefore, the surface makes semiconductors with different properties. Still, the surface variations on bulk materials, such as a wafer, are easy to ignore due to the fact that the long-range periodic structure of the surface will dilute the surface effect. In the previous experimental measurement, it was found that the intrinsic silicon (111) has better conductivity[12] and a lower trap state[13] between the conduction band and valance band than (110) and (100). Moreover, the merge of the conduction band and valance band within the Si(111) three-layer structure might be the reason.[14] For further discussing the surface band structure variation effect, Ge[15] and GaAs[16] were investigated, and we found out that this is a general effect in every semiconductor. The surface conductivity and surface trap states exist in different facets of Ge[17] and GaAs.[18] By revealing the detailed mechanism on the silicon (111) surface, this research focused on one layer and two layers of Si(111) plane structures and found out that they have metallic properties by the calculation results of electrical conductivities, and the band gap will merge and disappear at ⟨111⟩. This is the first time to release the precise mechanism for the metallic reason and values of one and two layers of Si(111) plane structures. Since the one layer and two layers of Si(111) plane structures are metallic, the nanodevice design on the Si wafer, with or without doping, will have clear guidance to avoid the surface issue. Moreover, the Si(111) surface plane is expected in the silicon wafer manufacturing process due to the lowest etching rate. The (111) plane is the close-packed silicon, and it is easy to retain the (111) plane after various wet etching processes in the semiconductor manufacturing process. The surface issue might be a minor issue for large-scale devices but a significant issue for ultrasmall devices. Since silicon is the most crucial semiconductor material globally, the metallic (111) plane structure needs to be revealed and reported. The dynamically

Received: November 23, 2021
Accepted: January 21, 2022
Published: February 2, 2022

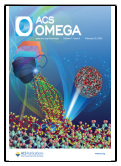

https://doi.org/10.1021/acsomega.1c06614
ACS Omega 2022, 7, 5385−5392

unstable structures of 1, 2, 4, 5, 7, 8, 10, and 11 layers of Si(111) structures might exist on the bulk material of Si and form the surface; thus, their dynamic instability might be varied by creating and deleting the surface dangling bond. Thus, the dynamically unstable surface structures [1, 2, 4, 5, 7, 8, 10, and 11 layers of Si(111)] will exist, and their unique band structure will influence the semiconductor properties of the Si material.

RESULTS AND DISCUSSION

The detailed discussion of the Si(111) surface properties by DFT calculations must establish the Si(111) surface structures with different layers. Figure 1a−l demonstrates the 1−12 layers

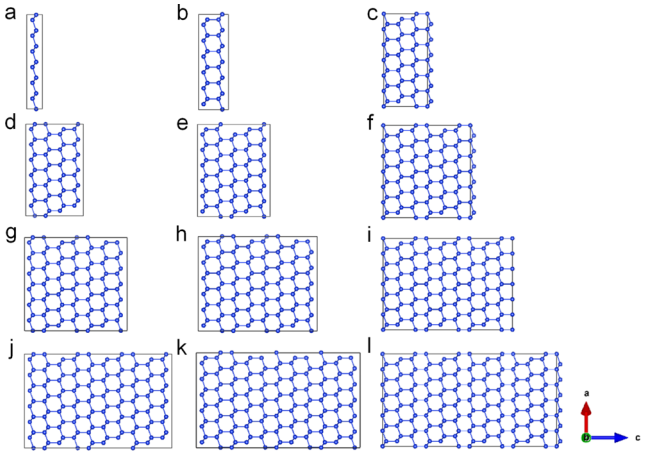

Figure 1. Original Si(111) plane slabs of 1−12 layers: (a) 1 layer, (b) 2 layers, (c) 3 layers, (d) 4 layers, (e) 5 layers, (f) 6 layers, (g) 7 layers, (h) 8 layers, (i) 9 layers, (j) 10 layers, (k) 11 layers, and (l) 12 layers.

by setting the slabs, and the 1−12 layers of Si(111) are all put into the cells. The 3 × 3 × 3 supercell of Si was used to slice out the slabs. The detailed information, as atomic position and cell parameters, of the structures in Figure 1a−l is listed in the Supporting Information. For reducing the calculation consumption and increasing the band structure result precision, the calculation needs to find out the symmetry structures for those slabs in Figure 1a−l by raising symmetry and processing the geometry optimization by the GGA-PBEsol approach. The optimization structures of Si(111), 1−12 layers, are shown in Figure S1a−l, and the detailed information, as atomic position and cell parameters, of the structures in Figure 1 and Figure S1a−l is listed in the Supporting Information. In Figure S1a−l, the different layers of Si(111) are transformed into simple structure units based on their crystal symmetry in Figure 1a−l, and these simplification units will be used to continue to process the calculations of band structures. The listing of these Si(111) layer structures in detail, in the Supporting Information, is prepared for the researchers to establish the structures and make the calculation independently.

The hybrid functional HSE06 calculated the band structures of Si(111) 1−12 layers, and the result is shown in Figure 2a−l. The 3 layers (Figure 2c), 6 layers (Figure 2f), 9 layers (Figure 2i), and 12 layers (Figure 2l) of Si(111) have the typical Si band structure with the indirect 1.17 eV band gap, which is the same band gap value for silicon at 0 K. Indeed, the raised symmetry structures in Figure S1c,f,i,l are the same structures as the silicon diamond cubic crystal structure, and this indicates that the silicon (111) has a periodicity with a three-layer structure that will become the standard cubic $Fd\bar{3}m$ space group. The DFT calculations set up the temperature at 0 K and prove that HSE06 is a proper function for the Si and Si-related structures in electronic structure calculations. The one layer of Si(111) in Figure 2a has no band gap, obviously with the conduction band connected to the valance band at the ⟨111⟩ direction. This conduction band and valance band connection behavior happens on all of the 2 layers (Figure 2b), 4 layers (Figure 2d), 5 layers (Figure 2e), 7 layers (Figure 2g), 8 layers (Figure 2h), 10 layers (Figure 2j), and 11 layers (Figure 2k) of Si(111).

The density of states (DOSs) of Si(111) from 1 to 12 layers are shown in (Figure S2a−l), and the 3 layers (Figure S2c), 6 layers (Figure S2f), 9 layers (Figure S2i), and 12 layers (Figure S2l) of Si(111) have the standard band gap as 1.17 eV. The contiguous states between the upper conduction band and the lower valence band are apparent within the 1 layer (Figure S2a), 2 layers (Figure S2b), 4 layers (Figure S2d), 5 layers (Figure S2e), 7 layers (Figure S2g), 8 layers (Figure S2h), 10 layers (Figure S2j), and 11 layers (Figure S2k) of Si(111). The electronic structures, band structures, and DOSs of Si(111) layers show semiconductor band gap properties with a three-layer periodicity. More calculation results need to discuss the three-layer periodicity of Si(111).

Furthermore, the structure stabilities of the Si(111) 1−12 layers are calculated by GGA−PBE in DFT for the phonon dispersion in Figure 3a−l and phonon DOSs in Figure S3a−l. The 3 layers (Figure 3c), 6 layers (Figure 3f), 9 layers (Figure 3i), and 12 layers (Figure S3l) of Si(111) are dynamic stable structures, according to the phonon dispersion diagrams. However, the 1 layer (Figure 3a), 2 layers (Figure 3b), 4 layers (Figure 3d), 5 layers (Figure 3e), 7 layers (Figure 3g), 8 layers (Figure 3h), 10 layers (Figure 3j), and 11 layers (Figure 3k) of Si(111) show dynamically unstable structures and properties by the negative phonon frequency vibrations in the phonon dispersion diagrams. Normally, the fact that more phonons vibrate with a negative frequency means that the structure is more dynamically unstable and indicates that this is not a stable phase.[19,20] For the detailed comparison of the structure stability, the phonon DOSs are shown in Figures S3a,b,d,e,g,h,j,k, and the contribution of imaginary (negative) frequency phonon DOSs the total phonon DOSs could be an index for dynamic stability. The fact that the structure has higher imaginary (negative) frequency phonon DOSs means lower dynamic stability. Indeed, the contributions of imaginary (negative) frequency phonon DOSs for Si(111) 1−12 layers are 15.70% (1 layer), 8.95% (2 layers), 0% (3 layers), 8.85% (4 layers), 3.53% (5 layers), 0% (6 layers), 5.21% (7 layers), 2.20% (8 layers), 0% (9 layers), 3.85% (10 layers), 1.60% (11 layers), and 0% (12 layers).

From the lower to higher layers of Si(111), the contribution of imaginary phonon DOSs is getting lower and lower. This indicates that the Si(111) one-layer and two-layer dynamic instability will be diluted when the dynamically stable three-layer periodic layer is added. Therefore, the 4 layers (as 3 layers plus 1 layer), 5 layers (as 3 layers plus 2 layers), 7 layers (as 6 layers plus 1 layer), 8 layers (as 6 layers plus 2 layers), 10 layers (as 9 layers plus 1 layer), and 11 layers (as 9 layers plus 2 layers) have lower imaginary phonon DOS parts. The periodic changes in the physical properties of the (111) plane caused by the three atomic layers do not exist. The one layer and two layers of Si(111) have metallic properties. Therefore, 3 times the number of layers plus 1 layer or 2 layers and 4, 5, 7, 8, 10, and 11 layers will gradually dilute the dynamic instability in Figure 3a−l. In addition, the metallicity may be diluted progressively as well. The dynamically unstable structure of 1, 2, 4, 5, 7, 8, 10, and 11

https://doi.org/10.1021/acsomega.1c06614
ACS Omega 2022, 7, 5385−5392

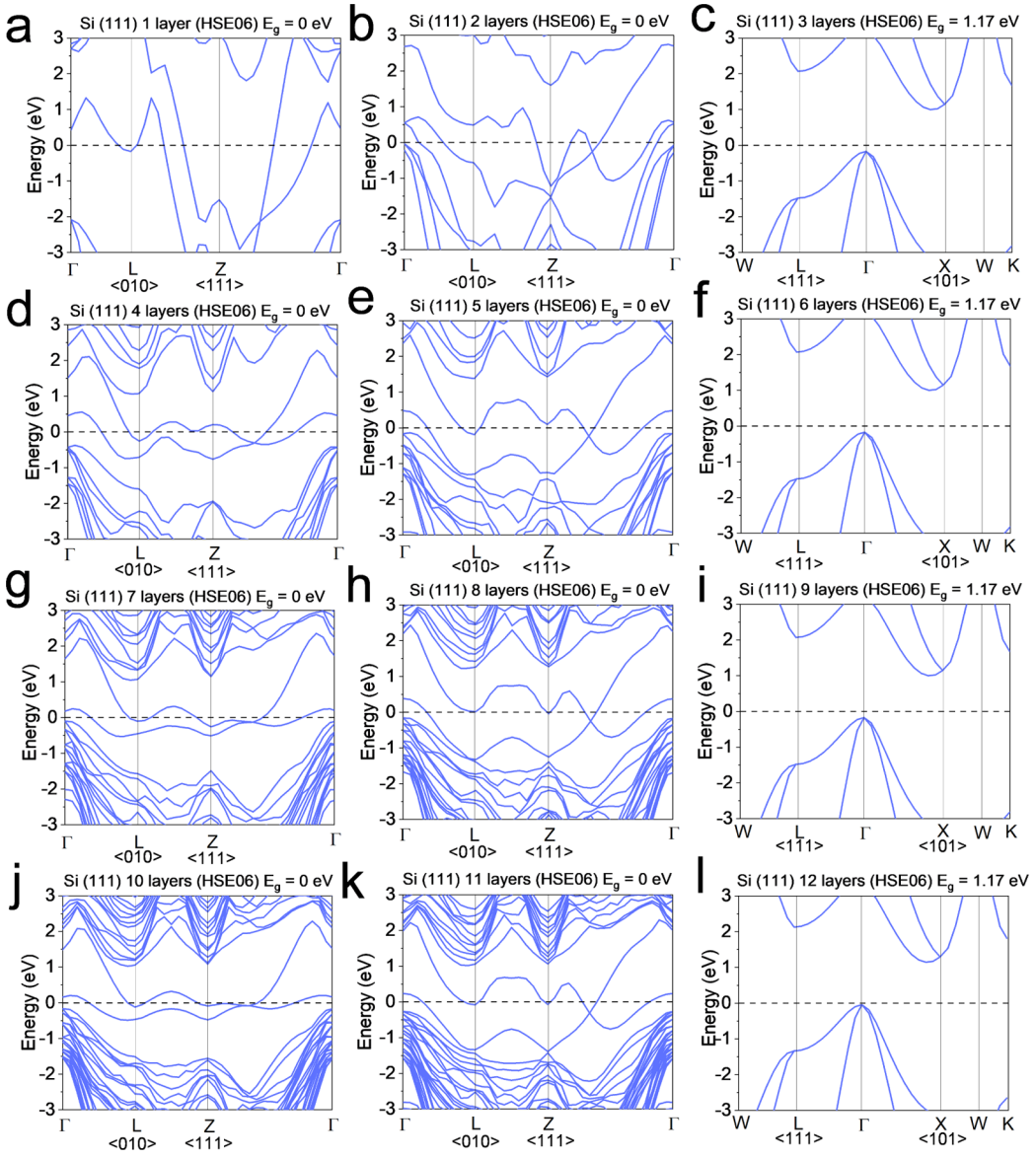

Figure 2. Band structure of the Si(111) plane slabs from 1−12 layers: (a) 1 layer, (b) 2 layers, (c) 3 layers, (d) 4 layers, (e) 5 layers, (f) 6 layers, (g) 7 layers, (h) 8 layers, (i) 9 layers, (j) 10 layers, (k) 11 layers, and (l) 12 layers.

layers of Si(111) structures might still exist in nature with a short phase existing timing, but they are easy to transform. If the dynamically unstable structure grows on the bulk material and forms the surface, their dynamic stability might be improved and influence the semiconductor properties. Therefore, it is important to investigate them.

The Si−Si bonding distortion on the Si(111) surface is the reason for the electronic structure and phonon DOS variation, as shown in Figures 2 and 3, and the mechanism within three layers of Si(111). For more structure information in detail, this research calculated the electron and X-ray diffraction (XRD) patterns of Si(111) 1−3 layers, as shown in Figure 4. The electron diffraction patterns of Si(111) for 1, 2, and 3 layers are shown in Figure 4a−c, and the zone axis is set as [111]. The electron diffraction patterns are different due to the Si−Si bonding distortion and could be observed from the Si(111) 1−3-layer structures by transmission electron microscopy, reflection high-energy electron diffraction, and low-energy electron diffraction. Therefore, the calculated electron diffraction patterns, by using the wavelength as 2.51 pm, of Si(111) in Figure 4a−c as 1−3 layers could be the reference for the surface suture distortion research of Si(111) and further identify the surface mechanism of the Si−Si bonding distortion on the Si(111) surface. The calculated XRD patterns, by using the wavelength as 1.54 Å, of Si(111) 1−3 layers are shown in Figure 4d−f, and the construction diffraction peaks are different due to the Si−Si bonding distortion.

The data indicate that the conduction band and valance band will connect in Si(111) one-layer and two-layer structures, as shown in Figure 2a,b. In addition, the detailed partial DOSs, by the contribution from Si 3s and 3p orbitals, of the Si unit cell, Si(111) one-layer structure, and Si(111) two-layer structure are shown in Figure 5a−c. For the Si unit cell in Figure 5a, the band gap is 1.17 eV, and the DOS in the valance band region is mainly contributed by the Si 3p orbital. Still, the contributions of 3s and 3p orbitals are equal in the conduction band region for the DOS. There is no band gap between the conduction band and valance band region for the Si(111) one-layer structure in Figure 5b. In

https://doi.org/10.1021/acsomega.1c06614
ACS Omega 2022, 7, 5385−5392

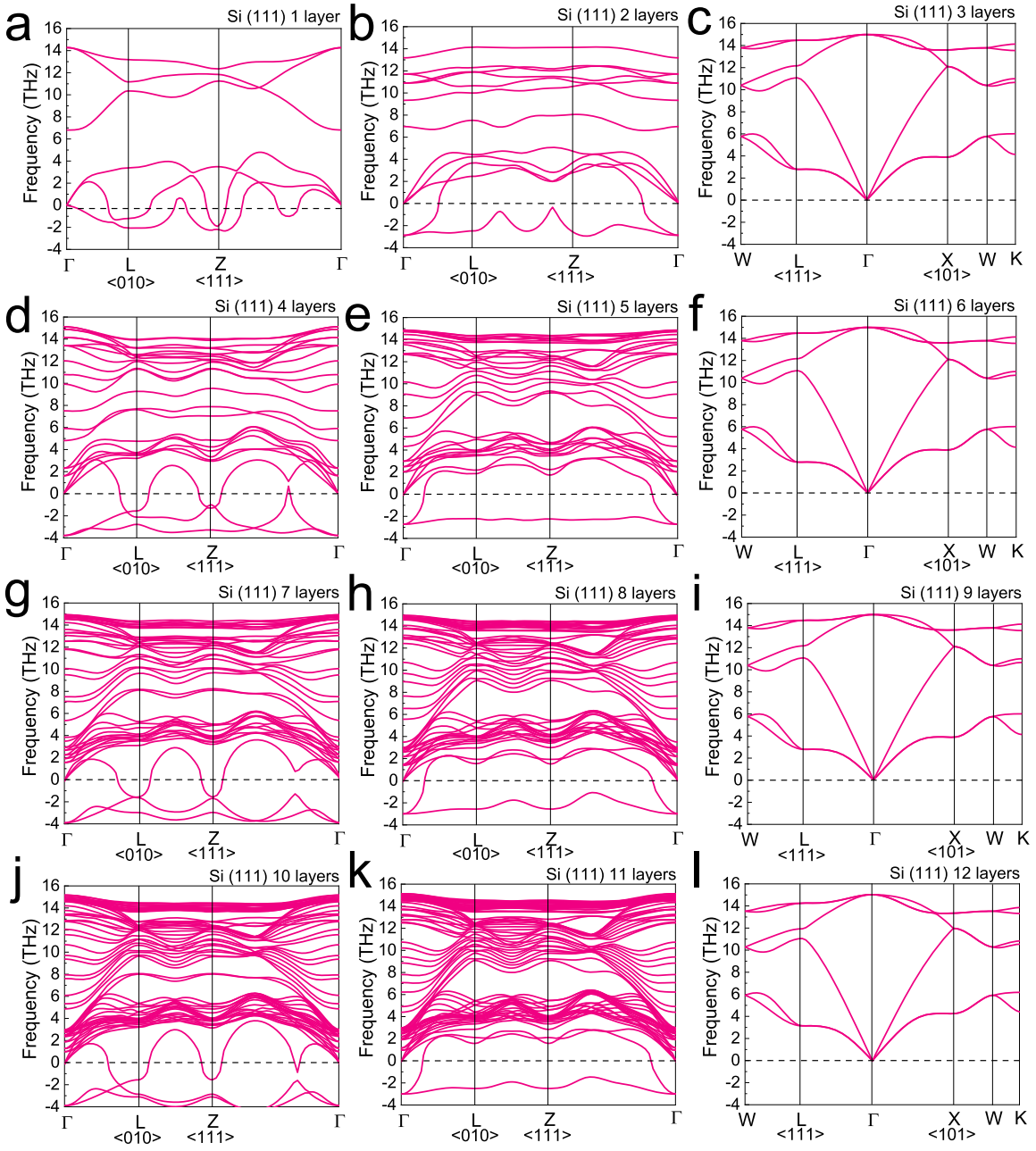

Figure 3. Phonon dispersions of Si(111) plane slabs from 1−12 layers: (a) 1 layer, (b) 2 layers, (c) 3 layers, (d) 4 layers, (e) 5 layers, (f) 6 layers, (g) 7 layers, (h) 8 layers, (i) 9 layers, (j) 10 layers, (k) 11 layers, and (l) 12 layers.

the valance band and conduction band, the density of the state is mainly contributed by the Si 3p orbital. The conduction band region with the 3p domination condition in the Si(111) one-layer structure differs from that in the Si unit cell. The previous research found that the zero band gap phenomenon is due to the uncommon Si−Si bonding distortion, from 2.34 to 2.253 Å.[14] The odd bonding distortion increases the 3p orbital contribution to the DOS, especially in the conduction band region. For the Si(111) two-layer structure in Figure 5c, the 3p orbital dominates the valance band DOS and is slightly higher than the 3s orbital in the conduction band region, with Si−Si bonding distorting to 2.331 Å.[14]

The ultrasmall device design could have a reference by DFT calculated from the electrical conductivity, carrier mobility, and carrier density about the Si(111) surface. Indeed, it will be helpful to understand the nano issue caused by the (111) surface layer by layer. Here, the calculated electrical conductivities, from 270 to 400 K, of the Si unit cell, Si(111) one-layer structure, and Si(111) two-layer structure are shown in Figure 5d, and the values are listed in Table 1. In Figure 5d, the Si(111) two-layer structure has higher electrical conductivities than the Si(111) one-layer structure and Si unit cell, and the Si(111) one-layer structure is more elevated than the Si unit cell for the temperature-dependent electrical conductivity. The calculated electrical conductivity of the Si unit cell at 300 K is 4.01×10^{-6} (Ω^{-1} cm^{-1}) in Table 1, and it is the same as the experimental result. Therefore, this research used a proper calculation method by DFT for Si and Si(111) surface estimation. In Table 1, the electrical conductivities of the Si(111) one-layer structure and two-layers structure are 129.68 (Ω^{-1} cm^{-1}) and 547.80 (Ω^{-1} cm^{-1}) at 300 K, respectively. Normally, the electrical conductivity of the metal at 300 K should be within 1 to 10^8

https://doi.org/10.1021/acsomega.1c06614
ACS Omega 2022, 7, 5385−5392

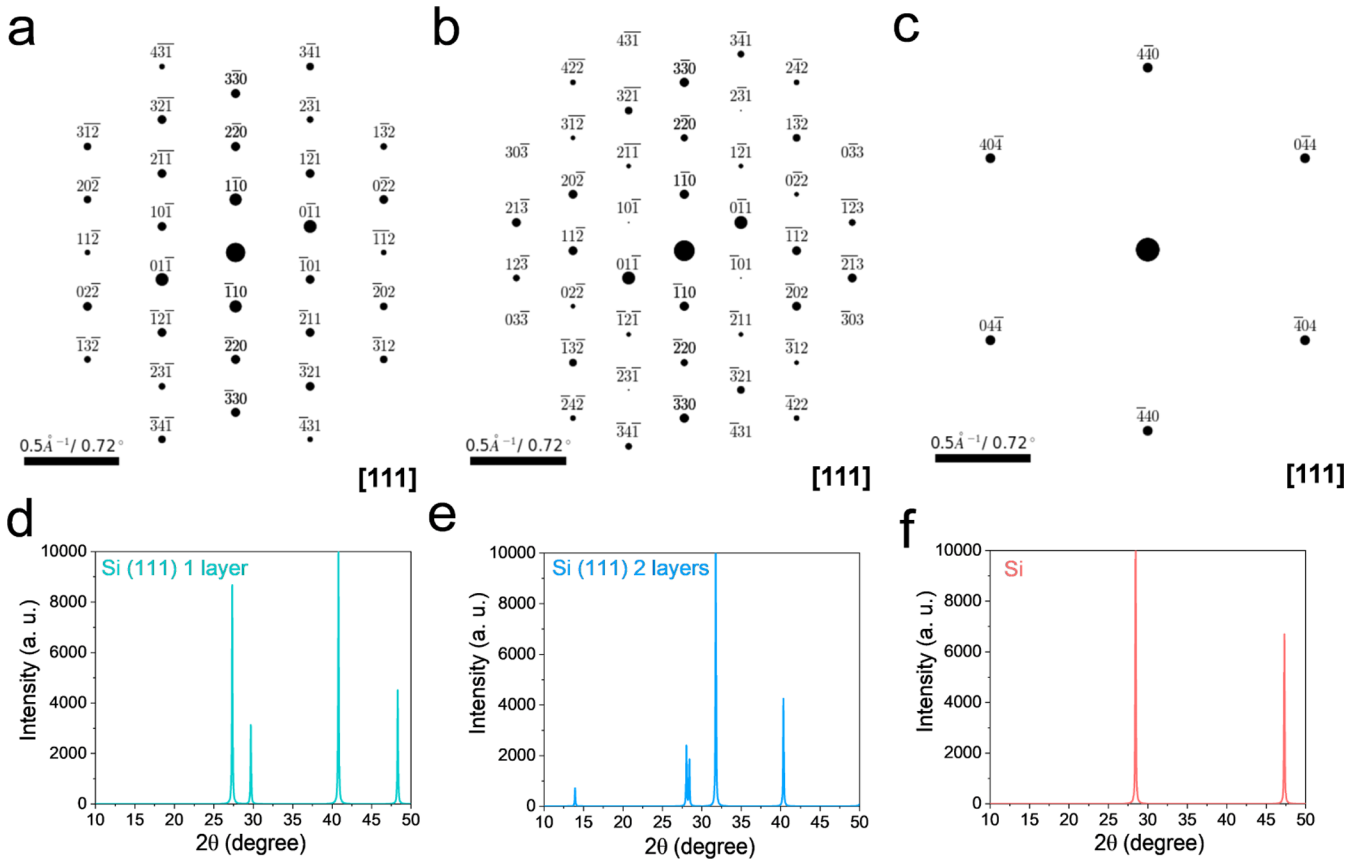

Figure 4. Calculated electron and XRD patterns of Si(111) plane slabs with different layers: (a−c) electron diffraction patterns of the Si(111) plane with one, two, and three layers and (d−f) XRD patterns of the Si(111) plane with one, two, and three layers.

(Ω^{-1} cm^{-1}). This research identifies that the Si(111) one-layer structure and two-layer structure are metals with metallic electrical conductivity. The (111) surface effect will influence the conductivity of Si and enhance the electrical conductivity by about 3.23×10^7 and 1.36×10^8 times for the Si(111) one-layer structure and two-layer structure, respectively.

For the temperature-dependent carrier mobility and carrier density of the Si unit cell, Si(111) one-layer structure, and Si(111) two-layer structure, the calculation results are shown in Figure 5e,f and listed in Tables 2 and 3 from 270 to 400 K. The Si unit cell structure has a low carrier mobility value in Figure 5e, which is mainly contributed by electrons from the positive value in the temperature-dependent carrier density diagram (Figure 5f). The Si(111) one-layer structure has higher carrier mobility than the other two structures, mainly contributed by holes from the negative value in the temperature-dependent carrier density diagram (Figure 5f). For the Si(111) two-layer structure, the carrier mobility value is highly negative and mainly contributed by electrons. In Table 2, the room-temperature carrier mobilities of the Si unit cell, Si(111) one-layer structure, and Si(111) two-layer structure are 10.78 (cm^2 V^{-1} s^{-1}), 0.54 (cm^2 V^{-1} s^{-1}), and −7.78 (cm^2 V^{-1} s^{-1}), respectively. Moreover, the room-temperature carrier densities of the Si unit cell, Si(111) one-layer structure, and Si(111) two-layer structure are -2.48×10^{19} (electron/cm^3), 2.60×10^{19} (electron/cm^3), and 2.32×10^{20} (electron/cm^3), respectively. For the carrier densities, the carrier of the Si unit cell is mainly contributed by the holes, and the electrons mainly contribute to the Si(111) one-layer and two-layer structures. Furthermore, the room temperature of molecular dynamics is calculated and shown in Figure S6a,b with the total potential energy variation of Si(111) 1−12 layer structures during the 6000 fs. The Si(111) 3-, 6-, 9-, and 12-layer structures have the same total potential energy, around −4100 kJ/mol. All the 12 structures could exist without sudden total potential energy drop within 6000 fs.

From 0 to 3000 K, the whole temperature range, temperature-dependent electrical conductivity, carrier mobility, and carrier density of the Si unit cell, Si(111) one-layer structure, and Si(111) two-layer structure are shown in Figure 5g−i. Different from the 270−400 K range in Figure 5d−f, the whole temperature range electrical conductivity, carrier mobility, and carrier density could offer a more comprehensive understanding of the fundamental properties within the Si unit cell, Si(111) one-layer structure, and Si(111) two-layer structure. For the whole temperature range electrical conductivity in Figure 5g, the Si unit cell has a value of nearly 0 at 0 K. Still, the Si(111) one-layer structure and Si(111) two-layer structure have electrical conductivities of a few hundreds at 0 K. This is another demonstration that the Si(111) one-layer structure and Si(111) two-layer structure have the metallic properties due to the fact that the semiconductor should have zero electrical conductivity at 0 K. In Figure 5h, the Si unit cell could not conduct at 0 K. The carrier mobility is 0 at 0 K. The metallic Si(111) one-layer structure and Si(111) two-layer structure have a higher and lower value than 0 at 0 K. For the cure profile of the Si unit cell in Figure 5h, it is consistent with general carrier mobility in the semiconductor material and convinces that the curves of the Si(111) one-layer structure and Si(111) two-layer structure are metallic carrier mobility curves.

https://doi.org/10.1021/acsomega.1c06614
ACS Omega 2022, 7, 5385−5392

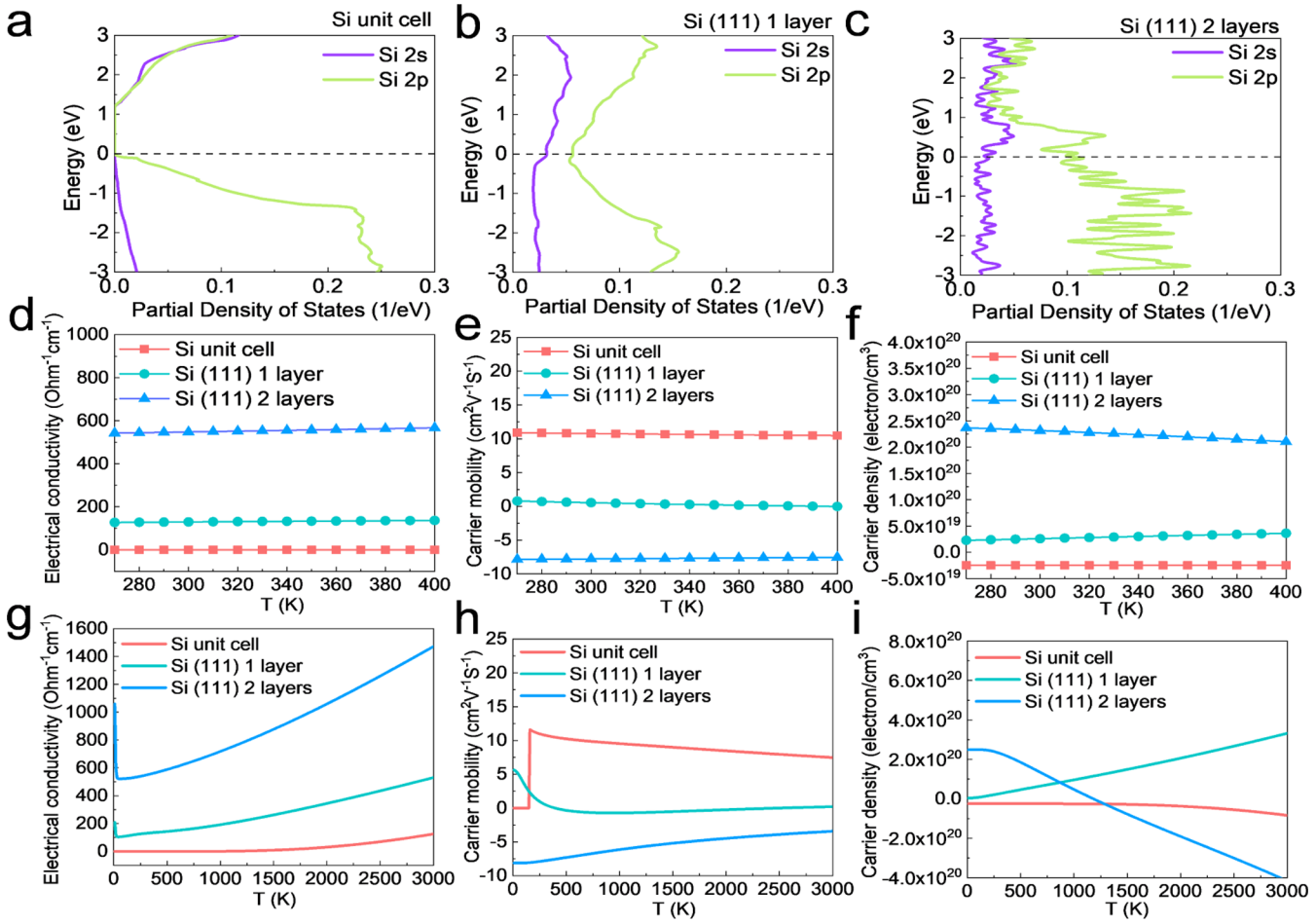

Figure 5. Partial DOSs (PDOSs), electrical conductivity, carrier mobility, and carrier density of the Si unit cell, the one-layer slab of (111), and two layers of (111). (a) PDOSs of the Si unit cell. (b) PDOSs of the Si(111) 1 layer. (c) PDOSs of Si(111) 2 layers. (d) Temperature-dependent electrical conductivity of the Si unit cell, one layer of (111), and two layers of (111) from 270 to 400 K. (e) Temperature-dependent carrier mobility of the Si unit cell, one layer of (111), and two layers of (111) from 270 to 400 K. (f) Temperature-dependent carrier density of the Si unit cell, one layer of (111), and two layers of (111) from 270 to 400 K. (g) Temperature-dependent electrical conductivity of the Si unit cell, one layer of (111), and two layers of (111) from 0 to 3000 K. (h) Temperature-dependent carrier mobility of the Si unit cell, one layer of (111), and two layers of (111) from 0 to 3000 K. (i) Temperature-dependent carrier density of the Si unit cell, one layer of (111), and two layers of (111) from 0 to 3000 K.

Table 1. Temperature-Dependent Electrical Conductivity Value List of the Si Unit Cell, One Layer of (111), and Two Layers of (111) from 270 to 400 K

T (K)	Si unit cell (Ω^{-1} cm^{-1})	Si(111) 1 layer (Ω^{-1} cm^{-1})	Si(111) 2 layer (Ω^{-1} cm^{-1})
270	7.04×10^{-7}	127.31	542.60
280	1.31×10^{-6}	128.13	544.30
290	2.33×10^{-6}	128.92	546.04
300	4.01×10^{-6}	129.68	547.80
310	6.68×10^{-6}	130.43	549.60
320	1.08×10^{-5}	131.15	551.42
330	1.70×10^{-5}	131.86	553.27
340	2.62×10^{-5}	132.55	555.15
350	3.94×10^{-5}	133.23	557.05
360	5.81×10^{-5}	133.90	558.97
370	8.40×10^{-5}	134.56	560.92
380	1.19×10^{-4}	135.22	562.89
390	1.67×10^{-4}	135.87	564.88
400	2.30×10^{-4}	136.52	566.89

Table 2. Temperature-Dependent Carrier Mobility Value List of the Si Unit Cell, One Layer of (111), and Two Layers of (111) from 270 to 400 K

T (K)	Si unit cell (cm^2 V^{-1} s^{-1})	Si(111) 1 layer (cm^2 V^{-1} s^{-1})	Si(111) 2 layer (cm^2 V^{-1} s^{-1})
270	10.90	0.79	−7.85
280	10.86	0.70	−7.82
290	10.82	0.62	−7.80
300	10.78	0.54	−7.78
310	10.74	0.47	−7.76
320	10.71	0.40	−7.73
330	10.68	0.34	−7.71
340	10.64	0.28	−7.69
350	10.61	0.22	−7.66
360	10.58	0.17	−7.64
370	10.55	0.12	−7.62
380	10.53	0.07	−7.59
390	10.50	0.03	−7.57
400	10.47	−0.02	−7.55

https://doi.org/10.1021/acsomega.1c06614
ACS Omega 2022, 7, 5385−5392

Table 3. Temperature-Dependent Carrier Density Value List of the Si Unit Cell, One Layer of (111), and Two Layers of (111) from 270 to 400 K

T (K)	Si unit cell (electron/cm^3)	Si(111) 1 layer (electron/cm^3)	Si(111) 2 layer (electron/cm^3)
270	-2.48×10^{19}	2.29×10^{19}	2.37×10^{20}
280	-2.48×10^{19}	2.39×10^{19}	2.35×10^{20}
290	-2.48×10^{19}	2.49×10^{19}	2.33×10^{20}
300	-2.48×10^{19}	2.60×10^{19}	2.32×10^{20}
310	-2.48×10^{19}	2.70×10^{19}	2.30×10^{20}
320	-2.48×10^{19}	2.80×10^{19}	2.28×10^{20}
330	-2.48×10^{19}	2.90×10^{19}	2.26×10^{20}
340	-2.48×10^{19}	3.00×10^{19}	2.24×10^{20}
350	-2.48×10^{19}	3.11×10^{19}	2.22×10^{20}
360	-2.48×10^{19}	3.21×10^{19}	2.19×10^{20}
370	-2.48×10^{19}	3.31×10^{19}	2.17×10^{20}
380	-2.48×10^{19}	3.41×10^{19}	2.15×10^{20}
390	-2.48×10^{19}	3.51×10^{19}	2.13×10^{20}
400	-2.48×10^{19}	3.62×10^{19}	2.10×10^{20}

CONCLUSIONS

In summary, the DFT calculation shows that the Si(111) one-layer structure and Si(111) two-layer structure have no band gap, and the conduction band and valance band connect toward the ⟨111⟩ direction. Thus, the 3p orbitals mainly contribute to the zero band gap of the Si(111) one layer and two layers in Si. Furthermore, this research found that the three-layer periodic variation on Si(111) in band gap variation is due to the Si(111) one-layer and two-layer addition on multiple layers from the stability realization in phonon dispersion diagrams of three. Moreover, the Si(111) one-layer structure and Si(111) two-layer structure belong to metallic properties with the electrical conductivities as 129.68 (Ω^{-1} cm^{-1}) and 547.80 (Ω^{-1} cm^{-1}) at 300 K, respectively. This research reveals the metallic silicon (111) plane structures in detail by using plenty of precise DFT results and making a breakthrough in nanosemiconductor research.

METHOD

The calculations were processed by VASP (Vienna ab initio Simulation Package)[21−23] with different exchange−correlation functionals for various purposes. GGA-PBEsol[24] processed the calculations for structure optimization with the default plane-wave cutoff energy set as 500 eV. A positive pressure would cause expansion during complete geometry optimization, and the maximum pressure setting of the process is −28.79 MPa. The electronic iteration convergence is 1×10^{-5} eV, the Gaussian smearing has a width of 0.05 eV, and the requested k-spacing for non-local exchange is $4 \times 4 \times 3$ mesh.

GGA−PBE[25,26] processed the calculations for phonon dispersion, phonon DOSs, molecular dynamics, and thermodynamic properties. For the detail setting of GGA−PBE, there is a default plane-wave cutoff energy set as 500 eV, the electronic iteration convergence is 1×10^{-5} eV using the blocked Davidson algorithm, the first-order Methfessel−Paxton smearing has a width of 0.2 eV, the linear-tetrahedron method with Blöchl corrections to the energy is used, and the requested k-spacing for non-local exchange is $8 \times 8 \times 9$ mesh. The molecular dynamics calculation is set as the micro canonical ensemble (nVE) at 298 K.

HSE06[27] processed the calculations for the band structure and the DOSs. For the detail setting of HSE06, there is a default plane-wave cutoff energy set as 500 eV. The electronic iteration convergence is 1×10^{-5} eV, the first-order Methfessel−Paxton smearing has a width of 0.2 eV, and the requested k-spacing for non-local exchange is $5 \times 5 \times 6$ mesh.

The semiconductor properties (electrical conductivity, carrier mobility, and carrier density, with the chemical potential set as 24 mu within 45 functions) were calculated within Boltzmann's transport theory, processed by HSE06, applying BoltzTraP based on the k-mesh and bands used for the Fermi surface above. The XRD and electron diffraction pattern calculations use the software Mercury and PTClab.

ASSOCIATED CONTENT

Supporting Information

The Supporting Information is available free of charge at https://pubs.acs.org/doi/10.1021/acsomega.1c06614.

Additional symmetric crystal structure, DOSs, phonon dispersion, and detailed crystal information of Si(111) layers (PDF)

AUTHOR INFORMATION

Corresponding Author

Chih Shan Tan − *Institute of Electronics, National Yang Ming Chiao Tung University, Hsinchu 30010, Taiwan;* orcid.org/0000-0001-9043-3237; Email: cstan@nycu.edu.tw

Complete contact information is available at: https://pubs.acs.org/10.1021/acsomega.1c06614

Author Contributions

C.S.T. initiated all the research ideas, performed calculations, and completed the paper writing independently.

Notes

The author declares no competing financial interest.

ACKNOWLEDGMENTS

This work was funded by the Ministry of Science and Technology of Taiwan (grants MOST 110-2636-E-009-020).

REFERENCES

(1) Poole, C. P.; Owens, F. J. *Introduction to Nanotechnology*; Wiley, 2003.

(2) *Springer Handbook of Nanotechnology*, 2nd rev. & extended ed.; Bhushan, B., Ed.; Springer, 2007.

(3) Williams, D. B.; Carter, C. B. The Transmission Electron Microscope. In *Transmission Electron Microscopy*; Springer: Boston, MA, 1996, pp 3−17. DOI: 10.1007/978-1-4757-2519-3_1.

(4) *Synchrotron Radiation: Basics, Methods and Applications*; Mobilio, S.; Boscherini, F.; Meneghini, C., Eds.; Springer, 2015.

(5) Wiesendanger, R. *Scanning Probe Microscopy and Spectroscopy: Methods and Applications*; Cambridge University Press, 1994.

(6) Hüfner, S. *Photoelectron Spectroscopy: Principles and Applications*; Springer Science & Business Media, 2013.

(7) Hussain, S.; Hussain, R.; Mehboob, M. Y.; Chatha, S. A. S.; Hussain, A. I.; Umar, A.; Khan, M. U.; Ahmed, M.; Adnan, M.; Ayub, K. Adsorption of Phosgene Gas on Pristine and Copper-Decorated B12N12 Nanocages: A Comparative DFT Study. *ACS Omega* **2020**, *5*, 7641−7650.

(8) Deng, Q.; Chai, J.-D. Electronic Properties of Triangle-Shaped Graphene Nanoflakes from TAO-DFT. *ACS Omega* **2019**, *4*, 14202−14210.

(9) Akdim, B.; Pachter, R. Bandgap Tuning of a (6,6) Boron Nitride Nanotube by Analyte Physisorption and Application of a Transverse

Electric Field: A DFT Study. *IEEE Trans. Nanotechnol.* **2011**, *10*, 1089−1092.
(10) Deng, S.; Zhang, Y.; Li, L. Strain Magnitude and Direction Effect on the Energy Band Structure of Hexagonal and Orthorhombic Monolayer MoS $_2$. *IEEE Trans. Nanotechnol.* **2018**, *17*, 419−423.
(11) Nishad, V. K.; Nishad, A. K.; Kaushik, B. K.; Sharma, R. First-Principle Analysis of Transition Metal Edge-Passivated Armchair Graphene Nanoribbons for Nanoscale Interconnects. *IEEE Trans. Nanotechnol.* **2021**, *20*, 92−98.
(12) Tan, C.-S.; Hsieh, P.-L.; Chen, L.-J.; Huang, M. H. Silicon Wafers with Facet-Dependent Electrical Conductivity Properties. *Angew. Chem.* **2017**, *129*, 15541−15545.
(13) Tan, C.-S.; Zhao, Y.; Guo, R.-H.; Chuang, W.-T.; Chen, L.-J.; Huang, M. H. Facet-Dependent Surface Trap States and Carrier Lifetimes of Silicon. *Nano Lett.* **2020**, *20*, 1952−1958.
(14) Tan, C.-S.; Huang, M. H. Metal-like Band Structures of Ultrathin Si {111} and {112} Surface Layers Revealed through Density Functional Theory Calculations. *Chemistry* **2017**, *23*, 11866−11871.
(15) Tan, C.-S.; Huang, M. H. Density Functional Theory Calculations Revealing Metal-like Band Structures for Ultrathin Germanium (111) and (211) Surface Layers. *Chem.—Asian J.* **2018**, *13*, 1972−1976.
(16) Tan, C. S.; Huang, M. H. Density Functional Theory Calculations Revealing Metal-like Band Structures and Work Function Variation for Ultrathin Gallium Arsenide (111) Surface Layers. *Chem.—Asian J.* **2019**, *14*, 2316−2321.
(17) Tan, C.-S.; Lu, M.-Y.; Peng, W.-H.; Chen, L.-J.; Huang, M. H. Germanium Possessing Facet-Specific Trap States and Carrier Lifetimes. *J. Phys. Chem. C* **2020**, *124*, 13304−13309.
(18) Tan, C.-S.; Chen, L.-J.; Huang, M. H. Large Facet-Specific Built-in Potential Differences Affecting Trap State Densities and Carrier Lifetimes of GaAs Wafers. *J. Phys. Chem. C* **2020**, *124*, 21577−21582.
(19) Leonov, I.; Poteryaev, A. I.; Anisimov, V. I.; Vollhardt, D. Calculated phonon spectra of paramagnetic iron at theα-γphase transition. *Phys. Rev. B: Condens. Matter Mater. Phys.* **2012**, *85*, 020401.
(20) Togo, A.; Tanaka, I. First principles phonon calculations in materials science. *Scr. Mater.* **2015**, *108*, 1−5.
(21) Kresse, G.; Furthmüller, J. Efficient iterative schemes forab initiototal-energy calculations using a plane-wave basis set. *Physical review. B, Condensed matter* **1996**, *54*, 11169−11186.
(22) Kresse, G.; Hafner, J. Ab initiomolecular dynamics for liquid metals. *Physical review. B, Condensed matter* **1993**, *47*, 558−561.
(23) Kresse, G.; Furthmüller, J. Efficiency of ab-initio total energy calculations for metals and semiconductors using a plane-wave basis set. *Comput. Mater. Sci.* **1996**, *6*, 15−50.
(24) Csonka, G. I.; Perdew, J. P.; Ruzsinszky, A.; Philipsen, P. H. T.; Lebègue, S.; Paier, J.; Vydrov, O. A.; Ángyán, J. G. Assessing the performance of recent density functionals for bulk solids. *Phys. Rev. B: Condens. Matter Mater. Phys.* **2009**, *79*, 155107.
(25) Perdew, J. P.; Burke, K.; Ernzerhof, M. Generalized Gradient Approximation Made Simple. *Phys. Rev. Lett.* **1996**, *77*, 3865−3868.
(26) Perdew, J. P.; Burke, K.; Ernzerhof, M. Generalized Gradient Approximation Made Simple [Phys. Rev. Lett. 77, 3865 (1996)]. *Phys. Rev. Lett.* **1997**, *78*, 1396.
(27) Krukau, A. V.; Vydrov, O. A.; Izmaylov, A. F.; Scuseria, G. E. Influence of the exchange screening parameter on the performance of screened hybrid functionals. *J. Chem. Phys.* **2006**, *125*, 224106.

https://doi.org/10.1021/acsomega.1c06614
ACS Omega 2022, 7, 5385−5392